Translational Oncology 55 (2025) 102365

Contents lists available at ScienceDirect

Translational Oncology

journal homepage: www.elsevier.com/locate/tranon

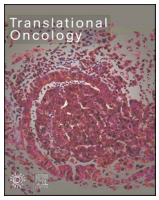

In-vitro immune-modulation of triple-negative breast cancer through targeting miR-30a-5p/MALAT1 axis using nano-PDT combinational approach

Asmaa Ramzy [a], Mohammad Abdel-Halim [b], Tamer Manie [c], Noha M. Elemam [d,e], Samar Mansour [a,f], Rana A. Youness [g,1,*], Aya Sebak [a,1,*]

[a] *Department of Pharmaceutical Technology, Faculty of Pharmacy & Biotechnology, The German University in Cairo, New Cairo 11835, Egypt*
[b] *Department of Pharmaceutical Chemistry, Faculty of Pharmacy & Biotechnology, The German University in Cairo, New Cairo 11835, Egypt*
[c] *Department of Breast Surgery, National Cancer Institute, Cairo University, Cairo, Egypt*
[d] *Clinical Sciences Department, College of Medicine, University of Sharjah, Sharjah 27272, United Arab Emirates*
[e] *Research Institute for Medical and Health Sciences, University of Sharjah, Sharjah, United Arab Emirates*
[f] *Faculty of Pharmaceutical Engineering, German International University (GIU), New Administrative Capital, Cairo 11835, Egypt*
[g] *Department of Molecular Biology and Biochemistry, Molecular Genetics Research Team (MGRT), Faculty of Biotechnology, German International University (GIU), New Administrative Capital, Cairo 11835, Egypt*

A R T I C L E I N F O

Keywords:
Tumor microenvironment
PDT
TNBC
Nanomaterials
MALAT1
Immunotherapy
miR-30a-5p
PD-L1
MIF
IL-10

A B S T R A C T

Background: Triple negative breast cancer (TNBC) is an immunogenic tumor; however, its tumor immune microenvironment (TIME) is densely packed with immune suppressive cytokines and immune checkpoints. The immune-suppressive features of TNBC TIME represent a considerable obstacle to any immunotherapeutic approach. The objective of this study was to develop a multimodal *in-vitro* strategy to manipulate the TNBC TIME and enhance patients' outcomes by employing carefully tailored hybrid chitosan-lipid Nanoparticles (CLNPs), metformin and chlorin e6 (Ce-6)-mediated PDT, alone or combined. Special focus is directed towards evaluation of the role of the selected treatment agents on the non-coding RNAs (ncRNAs) involved in tuning the immuno-oncogenic profile of TNBC, for instance, the miR-30a-5p/MALAT1 network.

Methods: This study enrolled 30 BC patients. CLNPs and ce-6-loaded CLNPs with different physicochemical features were synthesized and optimized using ionotropic gelation. The intracellular concentration and effects on MDA-MB-231 cellular viability were investigated. UHPLC was used to quantify ce-6. MDA-MB-231 cells were transfected with miR-30a-5p oligonucleotides and MALAT1 siRNAs using lipofection to investigate the interaction between MIF, PD-L1, TNF-α, IL-10, and the miR-30a-5p/MALAT1 ceRNA network. qRT-PCR was used to evaluate IL-10, TNF-α, and MIF expression levels, whereas flow cytometry was used for PD-L1.

Results: Immunophenotyping of BC biopsies revealed significantly elevated levels of immunosuppressive markers, including IL-10, TNF-α, PD-L1, and MIF in BC biopsies compared to its normal counterparts. Upon patient stratification, it was shown that MIF and IL-10 are upregulated in TNBC patients compared to non-TNBC patients. Nonetheless, immune suppressive biomarkers expression investigated in the current study was generally correlated with signs of poor prognosis. CLNPs with mean particle size ranging from 50-150 nm were obtained. CLNPs exhibited different patterns of intracellular uptake, cytotoxicity and modulation of the immunosuppressive markers based on their physicochemical properties and composition. In particular, CLNP4 *in-vitro* effectively reduced IL-10, TNF-α, MIF, and PD-L1. Loading of Ce-6 into CLNP4 (Ce6-CLNPs) improved the *in-vitro* cytotoxic effects via PDT. In addition, PDT with Ce6-CLNP4 enhanced the expression of tumor-suppressive miR-30a-5p and decreased oncogenic lncRNA MALAT1 expression in MDA-MB-231 cells, suggesting a potential for modulating the TNBC immuno-oncogenic profile.

* Corresponding authors.
E-mail addresses: rana.youness21@gmail.com, rana.youness@giu-uni.de (R.A. Youness), aya.sebak@gmail.com (A. Sebak).
[1] + Equal Contribution.

https://doi.org/10.1016/j.tranon.2025.102365
Received 15 November 2024; Received in revised form 12 March 2025; Accepted 16 March 2025

Conclusion: This study demonstrated that CLNPs and Ce-6-mediated PDT can modulate several key immunosuppressive factors and the miR-30a-5p/MALAT1 axis in TNBC cells. These findings provide a rationale for further *in-vivo* investigation of this multimodal therapeutic strategy.

Introduction

Immunotherapy has become a promising therapeutic option for triple negative breast cancer (TNBC) aggressive subtype [1,2]. Current immunotherapeutic approaches used could potentially activate the immune system by either active vaccination with cancer vaccines or passive immunization with tumor-specific antibodies and immunological modulators such as immune checkpoint inhibitors (ICIs) or blockades (ICBs) [3,4]. However, TNBC cells have the potential to overexpress programmed death-ligand 1 (PD-L1), an immunological checkpoint protein and several other immune checkpoint proteins that contribute to TNBC cells' ability to evade the immune surveillance [5,6]. This alters the immunological homeostasis and reduces the capacity of T cells to eradicate cancer cells, leading to tumor immune evasion [7,8]. The major challenge in TNBC is the highly immunosuppressive nature of the tumor immune microenvironment (TIME) [9,10] as defined by high levels of immunosuppressive cytokines such as interleukin 10 (IL-10), tumor necrosis factor alpha (TNF-α), and macrophage migration inhibitory factor (MIF) and altered extracellular matrix are all parts of the TIME, which all contribute to immune evasion and tumor promotion [11,12]. MIF is a pleiotropic cytokine that has been associated with higher levels of MDSCs and tumor angiogenesis [13,14]. TNF-α is a pro-inflammatory cytokine that has various and complex roles in tumorigenesis, including the promotion of tumor cell invasion [15–18] . IL-10, an immunosuppressive cytokine, has been associated with PD-1/PD-L1 signaling and advanced metastasis [19–22].

Given the limitations of single-target therapies in TNBC, a multimodal approach targeting PD-L1, MIF, TNF-α, and IL-10 in TNBC TIME is warranted. Non-coding RNAs (ncRNAs), including microRNAs (miRNAs) and long non-coding RNAs (lncRNAs) provide the solution to this dilemma, as they have become critical regulators of gene expression and multiple cellular processes [23–28]. In particular, miR-30a-5p, which can be a tumor suppressor or an oncomiR according to the context [29,30], has been reported to be involved in interaction with the oncogenic lncRNA MALAT1 associated with TNBC progression and metastasis [31–36].

Recently, studies have focused on developing alternate approaches to traditional immunotherapeutic drugs. Among many techniques, the employment of tailored biomaterials, medication repurposing, and photo-immunomodulation have gained increasing interest [37–39].

Photodynamic therapy (PDT) is one of the arising cancer therapeutic methods that have been identified as an invaluable tool in oncology [40,41]. PDT is made up of three key elements: photosensitizer (PS), light, and oxygen [42]. Choosing the right PS is one of the most important steps in PDT and is crucial for the most efficient and appropriate therapy [43]. Chlorin e6 (Ce6) is a second-generation PS, effectively halted the growth of the tumor by preventing cell division and inducing apoptosis [44]. Biomaterials, particularly chitosan-based nanoparticles (NPs), have shown immunomodulatory properties and can serve as drug delivery vehicles [45–50]. Hybrid chitosan-lipid nanoparticles (CLNPs) combine the advantages of polymeric and lipid-based formulations, such as biocompatibility and stability, improved drug payload, controlled drug release, long circulation time, hemo-compatibility, and better *in-vivo* efficacy [51–57]. Another interesting strategy is the repurposing of existing drugs, among which metformin represents one of the most used drugs in the treatment of type 2 diabetes with emerging anticancer properties [58–63].

Based on these findings, the primary goal of this *in-vitro* study is to develop a robust alternative multimodal immunotherapeutic approach for the treatment of TNBC. This approach compromises three therapeutic players; a PS with evident photo-immunomodulation effects (Ce6), properly tailored biomaterial hybrid to exert beneficial immunostimulatory effects (CLNPs) and a repurposed drug with growing evidence of positive impacts in BC (metformin). Given the evidence that therapies directed only at a single target have limitations, blocking multiple targets may be a better strategy for improving treatment outcomes in TNBC patients. To put this into practice, this study postulated that quadruple targeting of MIF, PD-L1, TNF- α and IL-10 in TNBC cells would activate the host anti-tumor immune response, thereby suppressing TNBC progression. Accordingly, a more specific goal is to investigate the potential of the proposed treatment modality to epigenetically attenuate the expression of these four immunosuppressive players; MIF, TNF-α, IL-10 and PD-L1 in TNBC. Considering the important role of ncRNAs in mediating the crosstalk between TNBC cells and the immune cells, more in-depth focus is directed towards evaluation of the potential role of the proposed treatment approach in regulating the miR-30a-5p/MALAT1 machinery in TNBC cells, hence providing a strong rationale for further studies in vivo.

Subjects, materials and methods

Subjects

Collection of breast tissues from BC patients

Breast biopsies were obtained from 30 female BC undergoing conservative mastectomy or lumpectomy procedures. Tumor tissues were removed from the tumor center, whereas non-cancerous tissues were extracted from 5- 7 cm safety margins surrounding the tumors. Pathological investigation confirmed the malignancy and normality of the tissues, and all patients received immunohistochemistry and pathological profiles, including Ki-67 expression level quatification. Smokers, male patients, and those with secondary malignancies were excluded. The average patient age was 47 years (range: 26 to 68). Tables S1 & S2 provide detailed clinical information about each patient. The study followed ethical guidelines, including clearance from the National Cancer Institute and the German University in Cairo (Ethical clearance Number: PTC-2020–10-SMH), and in accordance with the ethical standards of the declaration of Helsinki. All patients gave written informed consent.

Materials

Chitosan with a low molecular weight and Tripolyphosphate (TPP) were purchased from (Sigma-Aldrich, Germany). Soya lecithin was purchased from (ROTH, Germany). Sodium Fluorescein was purchased from (Lobachemie, India). Chlorin- e6 trisodium salt was purchased from (Apocare pharma,Germany). Metformin hydrochloride was purchased from (Sohan healthcare Pvt.Ltd, India). MDA-MB 231 (HTB-26) human triple negative breast cancer (TNBC) cell line was purchased from (ATCC, USA). The additional chemicals employed in this research were allof analytical grade.

Preparation and optimization of hybrid-chitosan lipid nanoparticle (CLNPs)

CLNPs were prepared by the ionotropic gelation method as previously reported, with some modifications [64]. For the formulation of CLNPs, two different solutions were separately prepared (chitosan, and polyanions). To obtain CLNPs of the desirable physicochemical properties, several variables including the pH of chitosan solution, the

composition and solvent type of the polyanions solution (cross-linker), and the polymer concentration have been investigated.

Briefly, low molecular weight chitosan was dissolved in 100 ml of 2 % acetic acid to prepare four different concentrations (1 mg/ml, 2 mg/ml, 5 mg/ml and 10 mg/ml). The prepared solutions were stirred at 300 rpm overnight at room temperature for complete solubilization of chitosan. Afterwards, the pH was adjusted to 4 or 5 using 1 N NaOH and the solutions were filtered using a syringe filter (0.45 μm, Millipore). For the preparation of the polyanions solution, 100 mg of lecithin with or without 100 mg TPP (±TPP) were dispersed in 5 ml deionized water or 50 % ethyl alcohol, then heated in water bath adjusted at 80°C. A mixture of 100 μl deionized water or sodium fluorescein solution or ce-6 tri sodium salt (1 mg/ml) was combined with variable volumes of the polyanions solution and deionized water for the preparation of cargo-free, fluorescein-loaded CLNPs, and ce-6CLNPs respectively. The resulting CLNPs were stirred for 30 min, centrifuged, reconstituted in deionized water (4 mg/ml), and stored at 4 °C until further analysis. Following a series of trials, seven CLNP formulations were selected according to three criteria; small particle size (<150 nm), low PDI (<0.5) and high reproducibility ≥ 85 %. The detailed composition of the selected formulations is shown in (Table S3). The composition of the other formulations is available in the supplementary materials in (Table S4). Out of these seven-cargo free CLNPs formulations prepared, one formulation was selected and loaded with Ce6 (Table S5).

Characterization of cargo free & medicated CLNPs

The hydrodynamic diameter (HD), polydispersity index (PDI), and surface charge of CLNPs & ce-6CLNPs were assessed as reported earlier [65]. Briefly, each nanoformulation, diluted 10-fold in ultra-pure water, was examined using a Zetasizer Nano-ZS (633 nm, He-Ne laser) from Malvern Instruments (UK). Particle size and polydispersity were assessed at 20 °C using disposable cuvettes (DTS0012), the instrument took 120 s for the sample to settle before running 30 consecutive scans with automatic adjustments for optimal signal strength. Each CLNP batch was analyzed at least three times using this rigorous process. For surface charge analysis, the folded capillary cells (DTS1070) were utilized and the analysis settings were switched to automatic mode and the temperature was modified as needed. The instrument then performed multiple measurements for each sample, ranging from 10 to 30 runs without pauses, to ensure accurate data. Each batch of CLNPs underwent this analysis three separate times for consistency. Both analyses employed polystyrene latex as reference and water as dispersant, and all measurements were independently repeated three times for each batch. The CLNP and Ce-6CLNP morphology was investigated using scanning electron microscopy (SEM) (Carl Zeiss Supra 55 FE-SEM). The samples were mounted on aluminum stubs, air-dried and coated with gold at current intensity of 15 mA for 5 min in Hummer 8.0 sputtering system (Anatech, USA).

UHPLC-UV methods for the quantification of Ce6

Ce-6 was quantified using UHPLC-UV. ACQUITY UPLC H—Class system (Waters Corp., Milford, MA, USA) was used. It consisted of Acquity UPLC Sample Manager FTN autosampler, Acquity UPLC QSM quaternary pump, ACQUITY UPLC PDA eLambda detector. Acquity BEH C18 50 mm × 2.1 mm column (particle size, 1.7 μm) was utilized to separate analytes (Waters, Ireland). UV detection was made at $\lambda_{max=}$400 nm. Gradient elution was used with a flow rate of 400 μL/min. The solvent system consisted of water containing 0.1 % formic acid (A) and 0.1 % formic acid in acetonitrile (B). The percentage of B started at an initial of 5 % and maintained for 0.5 min, then increased up to 100 % during 5 min, kept at 100 % for 2 min, and flushed back to 5 % in 1 min. System operation and data acquisition were controlled using Mass Lynx 4.1 software (Waters).

Cell culture

Human TNBC cell line, MDA-MB-231 adherent cells were cultured in Dulbecco's modified Eagle's medium (DMEM) supplemented with 4.5g/L Glucose, L-Glutamine, 1 % Penicillin-Streptomycin and 10 % Fetal Bovine Serum (FBS) and incubated at 37 °C and 5 % CO_2. This medium is denoted later as complete DMEM [66].

Cellular viability assay

The cell viability was determined using the Zombie Violet™ Fixable Viability Kit (423,113, Biolgened, USA). To evaluate the impact of CLNPs, lecithin or chitosan on the viability of MDA-MB-231 cells, 2×10^4 cells were seeded in 24-well plates and incubated for 24 h. Cells were then treated for 48 h with various concentrations of CLNPs in a range of 0.1–1 mg/ml. Cells then were scraped, washed with PBS and stained with Zombie Violet dye (1:500) in the dark. Washing of cells was then performed twice using flow cytometry buffer (2 % v/v BSA, 2 mM EDTA, 2 mM NaN_3 in PBS). Finally, cells were suspended in the same buffer before sample acquisition by Novocyte Flow Cytometer (Acea Biosciences, USA) [67]. The half maximal inhibitory concentration (IC_{50}) was calculated using GraphPad Prism software 8.3 and was employed for molecular analyses. The experiment was repeated three times in triplicate each time. In the setting of PDT of MDA-MB-231 cells, dark and light control experiments were performed to determine non-cytotoxic range of concentrations of medicated NPs and range of energy fluence of red-LED respectively. A handmade LED board was utilized to produce monochromatic red light with a wavelength of 645± 3 nm at a power density of 164 mW/cm^2 for 40 s, adjusted and fixed at 5 cm into the underneath of 96-well plate. The power density (mW/cm2) and energy fluence were calculated according to (Energy Fluence (J/cm2) = power density (W/cm2) x time of exposure (*sec*) equation [68]. For Ce-6 activation, a power density of ≤ 200 mW/cm2 was used in our study to avoid thermal effects of irradiation [69,70].

In the dark control, cells were treated with Ce-6CLNPs (0.05 to 2 mg/ml) for 24 h then tested for the viability in absence of LED exposure. In the light control, cells were exposed to home-made LED irradiation at energy fluence of (3.3 to 9.9 J/cm^2), in absence of PS. In the PDT experiments, cells were treated with Ce-6CLNPs (0.05 to 2 mg/ml) for 24 h, then exposed to LED irradiation (6.6 J/cm^2) to assess the cytotoxicity of the combination of PS and light. For the evaluation of the efficacy of the combination of PDT with metformin, cells were simultaneously treated with a non-toxic concentration of metformin. A summary of the PDT experimental setup is shown in (Table 1).

Quantitative NP cellular uptake

To quantify the concentration of NPs in MDA-MB-231 cells, a non-cytotoxic concentration of fluorescein-loaded NPs (100 μg/mL) was utilized [55]. MDA-MB-231 cells were seeded at a density of 3×10^3 cells per well in 96-well plates and incubated for 24 h. Cells were then treated with the fluorescent CLNPs for 48 h. Aspiration of CLNP-containing media and washing of cells with PBS was performed. The fluorescence intensity of the intracellular CLNPs was measured using a plate reader set to exc: 494 nm em: 512 nm. For each type of

Table 1
A description of the PDT experimental setup.

Experiment Type	Light	PS	Metformin
Dark Control	–	+ (0.05 to 2 mg/ml)	+/-
Light Control	+ (0.05 to 2 mg/ml)	–	+/-
PDT	+ (6.6 J/cm^2)	+ (0.05 to 2 mg/ml)	+/-

CLNPs, a calibration curve was created by diluting the corresponding fluorescein-loaded CLNPs with the appropriate volume of complete DMEM in a series of dilutions. The intracellular concentration of CLNPs was then determined using the calibration curves.

Oligonucleotides transfection in MDA-MB-231 cells

MDA-MB-231 cells were transfected with oligonucleotides, including miR-30a-5p mimics (hsa-miR-30a-5p miRNA mimic Cat. No.: 219,600) and MALAT1 siRNAs (siRNA directed against human MALAT1 Cat # ID: SI03670541) acquired from Qiagen, Germany. Transfection experiments were performed in triplicate using HiPerfect Transfection Reagent (Qiagen, Germany).

Molecular analyses

Gene expression analysis by RT-qPCR

Total RNA was isolated from the control cells and cells treated with the IC_{50} of CLNPs, Ce-6CLNPs, chitosan or 1 mg/ml of lecithin using the TRIzol RNA extraction reagent (Applied Biosystems, USA). The High-Capacity cDNA Reverse Transcription (KitTaqMan® MicroRNA Reverse Transcription Kit) (Applied Biosystems, USA) was used for reverse transcription as directed by the manufacturer. TaqMan Real-Time q-PCR-StepOne™ Systems (Applied Biosystems, USA) were utilized to determine the relative expression of all targets. In this work, β-actin was used for the cell line and the housekeeping gene for BC tissues was the 18S rRNA expression assay. MIF (Hs00236988_g1), IL-10 (Hs00961622_m1), TNF-α (Hs00174128_m1), PD-L1 (Hs00204257_m1), eukaryotic18s rRNA (Cat #: 4319413E), and β-actin (Hs99999903_m1) mRNAs were reverse-transcribed and their relative expression was quantified. Relative expressions were calculated using the $2^{-\Delta\Delta CT}$ method [71–73]. . Each PCR reaction was performed in triplicate at least three times.

Immune checkpoint PD-L1 expression analysis by flow cytometry

For the evaluation of surface expression of the immune checkpoint PD-L1 by flow cytometry, 2×10^4 MDA-MB-231cells were seeded in 24-well plates and incubated for 24 h. Then cells were subjected to the IC_{50} concentrations of the CLNPs, ce-6CLNPs, chitosan or 1 mg/ml of lecithin for 48 h. Following the incubation, cells were scraped and rinsed twice with ice-cold PBS, and viability was assessed using the Zombie Viability Kit. Cells were stained with Brilliant Violet 785™ anti-human CD274 (B7-H1, PD-L1) Antibody (329,735, Biolegend) at a dilution of 1:200, and TruStain fcX-CD16/32 (101,319, Biolegend) at a dilution of 1:100 to prevent non-specific Fc receptors binding Following labelling. Then, samples were analyzed by Novocyte Flow Cytometer (Acea Biosciences, USA). For data analysis, FlowJo™ software was utilized [67].

Statistical analysis

Statistical analysis was done using the GraphPad Prism 8.3 software (San Diego, CA, USA). Results obtained from at least three independent experiments and data is presented as mean ± standard error of the mean (SEM). To compare the two independent groups, a non-parametric unpaired student-*t*-test was used. For multiple comparisons, a one-way analysis of variance (one-way ANOVA) followed by Tukey's post hoc analysis was used. The threshold of significance is denoted by ns; not significant, (*); p value <0.05, (**); p value <0.01, (***); p value <0.001, and (****); p value <0.0001.

Results

Group1: cargo free hybrid chitosan-lipid nanoparticles (CLNP1-CLNP7)

CLNPs exhibited different physicochemical properties according to their composition (C:L ratio)

Three inclusion criteria were employed to select formulations for further analyses: a particle size < 150 nm, a PDI < 0.5 and a high reproducibility ≥ 85 %. Seven formulations were found to fall into these inclusion criteria. These formulations were further ranked according to their C:L ratio and were given formulation codes CLNP1-CLNP7. Looking more closely at the physicochemical properties of the selected formulations, it could be observed that the particle size was demonstrated to be dependent on the C:L ratio as follows: increasing the C:L ratio from 1:10 to 1:5 resulted in no significant difference in particle size. However, a further increase in the C:L ratio to 1:1 and 2:1 resulted in a considerable drop in particle size, followed by an increase in particle size beyond 2:1. Regarding the surface charge of CLNPs, a trend of decrease in negativity and increase in positivity was observed as C:L ratio increases Table 2. The physicochemical properties of all other formulations are available in the supplementary materials in (Table S6). SEM imaging for morphological evaluation revealed spherical NPs with smooth surfaces and nanometric size distributions similar to those obtained by DLS using Malvern Zetasizer as shown in (Fig. 1A-G).

Neither the composition, nor the extent of intracellular uptake alone determine the effect of CLNPs on MDA-MB-231 viability

Upon evaluation of the cellular viability by flow cytometry, chitosan solution has demonstrated a significant toxicity to MDA-MB-231 cells with an IC_{50} of 0.02 ± 0.01 mg/ml (Fig. 1H and Table 3). In contrast, lecithin has been shown to be non-cytotoxic up to 1 mg/ml. Regarding CLNPs, they were observed to be less cytotoxic than chitosan and more than lecithin with a range of IC_{50} of 0.09–0.37 mg/ml. Cells were then treated with a non-cytotoxic concentration of fluorescein-loaded CLNPs for 48 h in order to determine whether the diversity of CLNPs cytotoxicity is dependent on the extent of NP internalization or not. CLNP1–3, which were similar in size (approximately 90 nm), showed no significant difference in their accumulation within MDA-MB-231 cells regardless of their composition (C:L ratio). Yet, CLNP2 showed the lowest IC_{50} of 0.06 ± 0.03 mg/ml which was approximately 6-fold more cytotoxic than CLNP1 (Fig. 1I). In the case of the 60-nm CLNP4 & CLNP5 and the 140-nm CLNP6 and CLNP7, a positive relationship between the intracellular concentration and cytotoxicity was observed. CLNP4 and CLNP7 which showed a 10- and 4-fold higher accumulation than CLNP5 and CLNP6, respectively, exhibited lower IC_{50} and hence higher cytotoxicity.

Chitosan, lecithin and CLNPs alleviate the immunosuppressive TME and the immune checkpoint signaling in TNBC

Expression profile of MIF, PD-L1, TNF-α and IL-10 in BC and TNBC patients

To evaluate the relevance of the selected biomarkers, the expression patterns of MIF, and PD-L1, in BC patients were initially investigated. When compared to normal tissues, MIF, and PD-L1, were found to be considerably up-regulated in BC patients Figure (2 A-B). Regarding the expression patterns of TNF-α and IL-10, previous studies have consistently demonstrated elevated levels of TNF-α and IL-10 in BC patients [10]. Upon patient stratification, it was shown that MIF (Fig. 2C) and IL-10 (Fig. 2D) were highly up-regulated in TNBC patients ($n = 10$) compared to non-TNBC patients ($n = 20$). Moreover, it was found that MIF is positively correlated with high Ki-67 (Fig. 2E) and lymph node metastasis (Fig. 2F). Yet, IL-10 (Fig. 2G) and TNF-α (Fig. 2H) correlated with bigger tumor size (>5cm).

CLNPs exhibited different impact on the immunosuppressive milieu and immune checkpoint signaling in TNBC cells

MDA-MB-231 cells were treated with the IC_{50} conditions of CLNPs,

Table 2
Physicochemical properties of the selected CLNPs. Particle size (expressed as z-average in nm), PDI and surface charge (expressed as zeta potential in mV) obtained by Malvern Zetasizer ($n = 3$).

Formulation code	CLNP1	CLNP2	CLNP3	CLNP4	CLNP5	CLNP6	CLNP7
Z-average (nm)	87 ± 9	94 ± 13	103 ± 6	65 ± 9	61 ± 6	143 ± 29	141 ± 13
PDI	0.22 ± 0.02	0.30 ± 0.03	0.39 ± 0.05	0.22 ± 0.02	0.37 ± 0.08	0.45 ± 0.12	0.41 ± 0.30
ζ-potential (mV)	−2.1 ± 0.2	−4.1 ± 0.7	−2.8 ± 0.6	14.0 ± 2.0	37.0 ± 0.0	40.0 ± 2.0	40.0 ± 2.0

chitosan or 1 mg/ml of lecithin. Results showed that the relative expression of MIF, PD-L1, TNF-α and IL-10 has been differently altered according to the status of chitosan or lecithin (free or formulated), and the physicochemical properties (size and composition).

In the case of MIF, none of the free components could alter its transcription level. However, a significant downregulation was observed with all the CLNPs which was more evident as C:L ratio increased in which CLNP6 and CLNP7 recorded the lowest levels of MIF expression (Fig. 3A). Regarding IL-10, both chitosan and lecithin solutions significantly downregulated its expression. However, there was no specific trend with regards to CLNPs. It could be observed that IL-10 was undetectable in the case of CLNP1 and CLNP2, unaltered in the case of CLNP3, significantly downregulated in the case of CLNP4, CLNP6 and CLNP7, but significantly upregulated in the case of CLNP5 (Fig. 3B). TNF-α expression was more predictable. It was found that chitosan caused a significant downregulation while lecithin had no effect on TNF-α expression. In the case of CLNPs, CLNP1 which possessed the highest content of lecithin did not alter TNF-α levels. On the contrary, all the other formulations which exhibited higher composition of chitosan and lower composition of lecithin resulted in a significant downregulation (Fig. 3C). Regarding the expression of the immune checkpoint protein (PD-L1), lecithin and chitosan produced opposite effects; whereas chitosan significantly lowered PD-L1 expression in contrary to lecithin (Fig. 3D). In the case of CLNPs, only the CLNPs of intermediate C:L ratio (CLNP3 and CLNP4) downregulated PD-L1 in contrary to CLNPs of low (CLNP1) and high (CLNP6 and CLNP7) C:L ratios. Whereas CLNP2 had no effect compared to the control.

Group 2: medicated Ce-CLNPS

Physicochemical properties of ce-6 CLNPs (PDT)

CLNP4 has a substantial advantage over the other formulations by demonstrating higher intracellular uptake and significant downregulation of MIF, PD-L1, TNF-α and IL-10. For such reason all of these previous results, CLNP 4 has been loaded with photosensitize (PS) ce-6 drug for further investigations. Table S7 implants the physicochemical features of ce-6 CLNPs.

Morphology of ce-6 CLNPs

SEM imaging for morphological evaluation revealed spherical NPs with smooth surfaces and nanometric size distributions similar to those obtained by DLS using Malvern Zetasizer as shown in Fig. 4.

Evaluation of encapsulation efficiency (EE) of ce-6 by UHPLC-UV method

Ce-6 in CLNP4 was indirectly determined by quantifying the unencapsulated fraction of the PS using UHPLC-UV as shown in Figure (S1A). A linear relationship has been established between the AUC and the concentration of ce-6 in the range of (0.5 to 10 μg/ml) and an encapsulation efficiency % (EE%) of ce-6 of 99.5 % was determined Figure (S1B).

Ce-6CLNPs - mediated PDT in monotherapy or in combination with metformin are similarly effective in MDA-MB-231

In the context of PDT, a dark control (PS, no light) and a light control (light, no PS) are warranted to select nontoxic concentration range of the PS and exposure conditions of the light source respectively (Fig. 4B and C). In the absence of light, ce-6CLNPs produced no cytotoxicity up to a concentration of 6 μg/mL in the presence or absence of metformin. Combining both PS and light (40 s) resulted in IC_{50} values of 3.6 ± 1.5 or 6.8 ± 1.4 μg/mL in the case of PDT monotherapy or the combination with metformin, respectively (Fig. 4D).

Investigating superiority of ce-6CLNPs (PDT) over CLNPs, metformin and co-treatment (PDT+ metformin) in relieving the immunosuppressive TME and immune checkpoint signaling in TNBC

In order to evaluate the efficacy of the proposed alternative therapy to conventional immunotherapy, the three selected players were evaluated; CLNP4 as immunomodulatory carrier, ce6-CLNP4 as a third generation PS for PDT and metformin as an example of repurposed drugs with anticancer and immunomodulatory potential. MDA-MB-231 cells were treated with the IC_{50} conditions of Ce-CLNPs and non-toxic concentration of metformin then MIF, TNF-α and IL-10 expression levels were assessed using RT-qPCR. Whereas single-parameter flow cytometry was employed to evaluate PD-L1 expression level. All the treatments showed a significant downregulation of MIF, PD-L1 TNF-α and IL-10 (Fig. 5A-D). The combination of nano-based PDT and metformin implying the three players resulted in a disappointment; in which less repression of all markers was observed. However, PDT monotherapy represented an advantage with regards to MIF (Fig. 5A) and PD-L1 (Fig. 5B). Interestingly, the CLNP4 showed the lowest levels of TNF-α (Fig. 5C), and IL-10 (Fig. 5D). Therefore, it could be noted that treating MDA-MB-231 with CLNP4 was sufficient for repressing their immunosuppressive nature by downregulating the expression levels TNF-α and IL-10. While adding PDT in the treatment protocol presented a further advantage in alleviating the cytokine storm by downregulating the expression of MIF and extended the effect to suppression of the immune checkpoint, PD-L1. However, a combination with metformin leads to deterioration with respect to all markers.

Ce-6 CLNPs (PDT) repress TNBC hallmarks by manipulating miR-30a-5p/MALAT-1 machinery

In a more comprehensive approach, this study explored the potential regulatory role of ce-6CLNPs (PDT) on ceRNAs network between miR-30a-5p and MALAT1 in the treatment of TNBC patients. Regarding the expression patterns of miR-30a-5p & MALAT-1, previous studies have consistently demonstrated that miR-30a-5p was significantly downregulated in BC patients compared to its normal counterparts while MALAT1 was found to be up-regulated compared to normal counterparts in BC patients [36,74].

To validate the impact of miR-30a-5p/MALAT1 machinery on the quadruple targets in this study, first, a forced expression of miR-30a-5p in MDA-MB-231 was performed using miR-30a-5p mimics. On the other hand, knocking down of MALAT1 was performed using MALAT1 siRNA. Results confirmed successful transfection; in which a significant upregulation of miR-30a-5p and downregulation of MALAT-1 were observed (Fig. 6A and B respectively). As a next step, the impact of miR-30a-5p on TNF- α and IL-10 transcript levels in MDA-MB-231 cell lines was evaluated. Ectopic expression of miR-30a-5p oligonucleotides resulted in a decreased TNF-α and IL-10 expression (Fig. 6C and D). Moreover, the interplay between miR-30a-5p and MALAT-1 has been established. In which miR-30a-5p mimics induced a significant downregulation of MALAT-1 (Fig. 6E). Furthermore, knocking down of MALAT-1 in TNBC cell lines resulted in a significant decrease in MIF and PDL1 transcript levels (Fig. 6F-G), while miR-30a-5p transcript level was upregulated compared to the respective mock cells (Fig. 6H). This further elaborates on the interaction between miR-30a-5p and MALAT-1 in a ceRNA

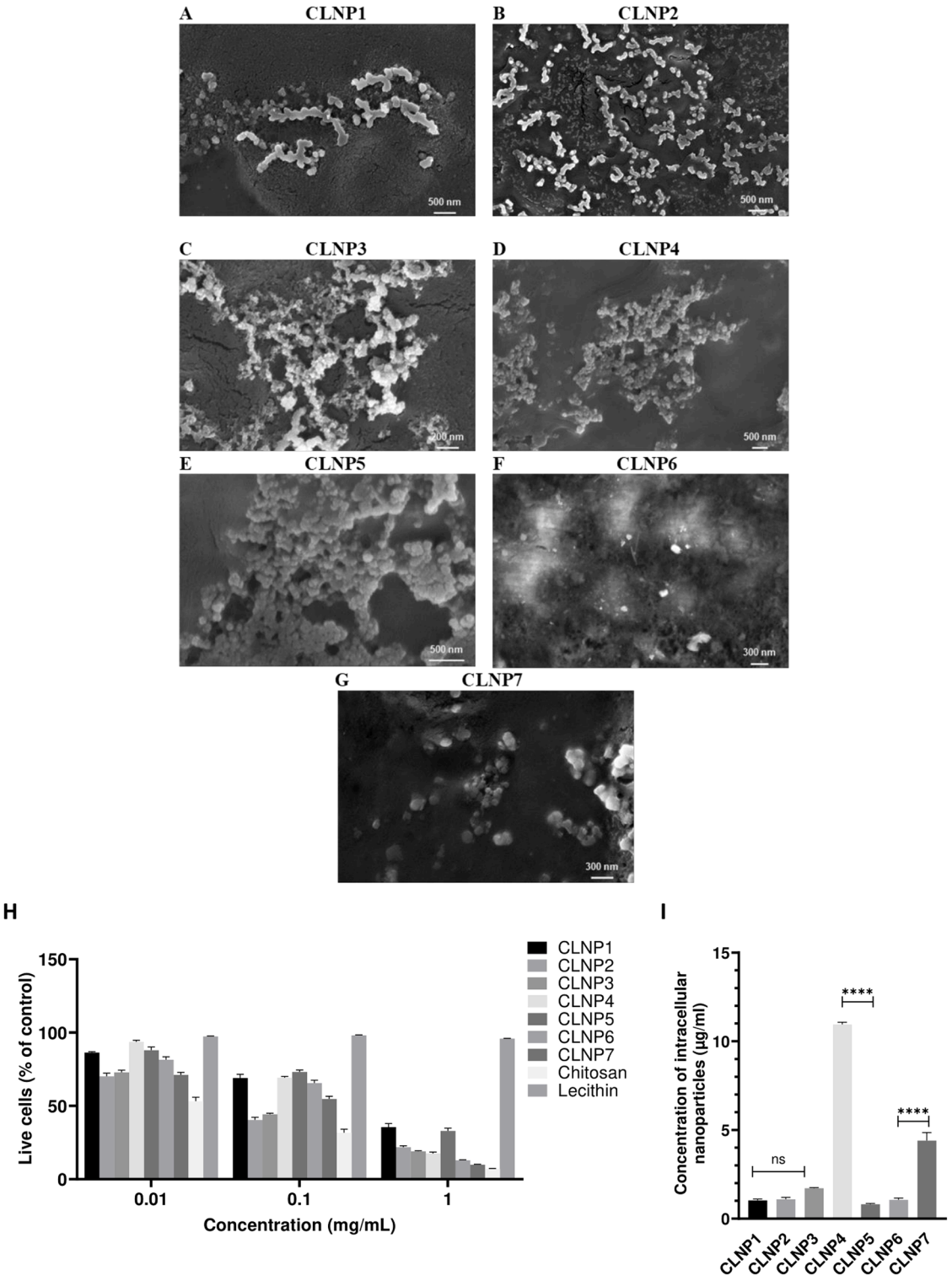

Fig. 1. Surface morphology,Cell viability,& intracellular uptake of the selected CLNPs. (A-G) SEM micrographs of CLNP1–7 by Carl Zeiss Supra 55 FE-SEM at electron high tension (EHT) of 5 kV and magnification 10–20 k x. Cell viabiltyof CLNPs H) Cell viability of CLNPs, chitosan and lecithin performed by flow cytometry using Zombie VioletTM Fixable Viability Kit. In each experimental run, the percentage of live cells from each treated sample was normalized to the average of the percentage of live cells from the control samples. The average of the replicates was then plotted as a single entry. (I) The concentration of intracellular CLNPs (µg/mL) obtained by measuring the fluorescence intensity of the fluorescently-labelled NPs.Statistical analysis was performed by one-way ANOVA followed by Tukey's post-hoc test using GraphPad Prism software 8.3, and data is expressed as mean ± SEM. ns; not significant, (****);p value <0.0001.

network. Finally, upon application of PDT using ce6-CLNP4 under IC_{50} conditions, a significant overexpression of miR-30a-5p was observed (Fig. 6I). On the contrary, MALAT-1 was significantly downregulated (Fig. 6J).

Discussion

TIME has been identified as one of the major causes of TNBC patients' immune resistance, being rampant with immune suppressive

Table 3
IC_{50} values of the selected CLNPs, chitosan, and lecithin in MDA-MB-231 cells following 48 h exposure.

Formulation code	CLNP1	CLNP2	CLNP3	CLNP4	CLNP5	CLNP6	CLNP7	Chitosan	Lecithin
IC_{50} (mg/mL)	0.35±0.12	0.06±0.03	0.07±0.03	0.22±0.01	0.37±0.09	0.16±0.04	0.09±0.03	0.02±0.01	>1

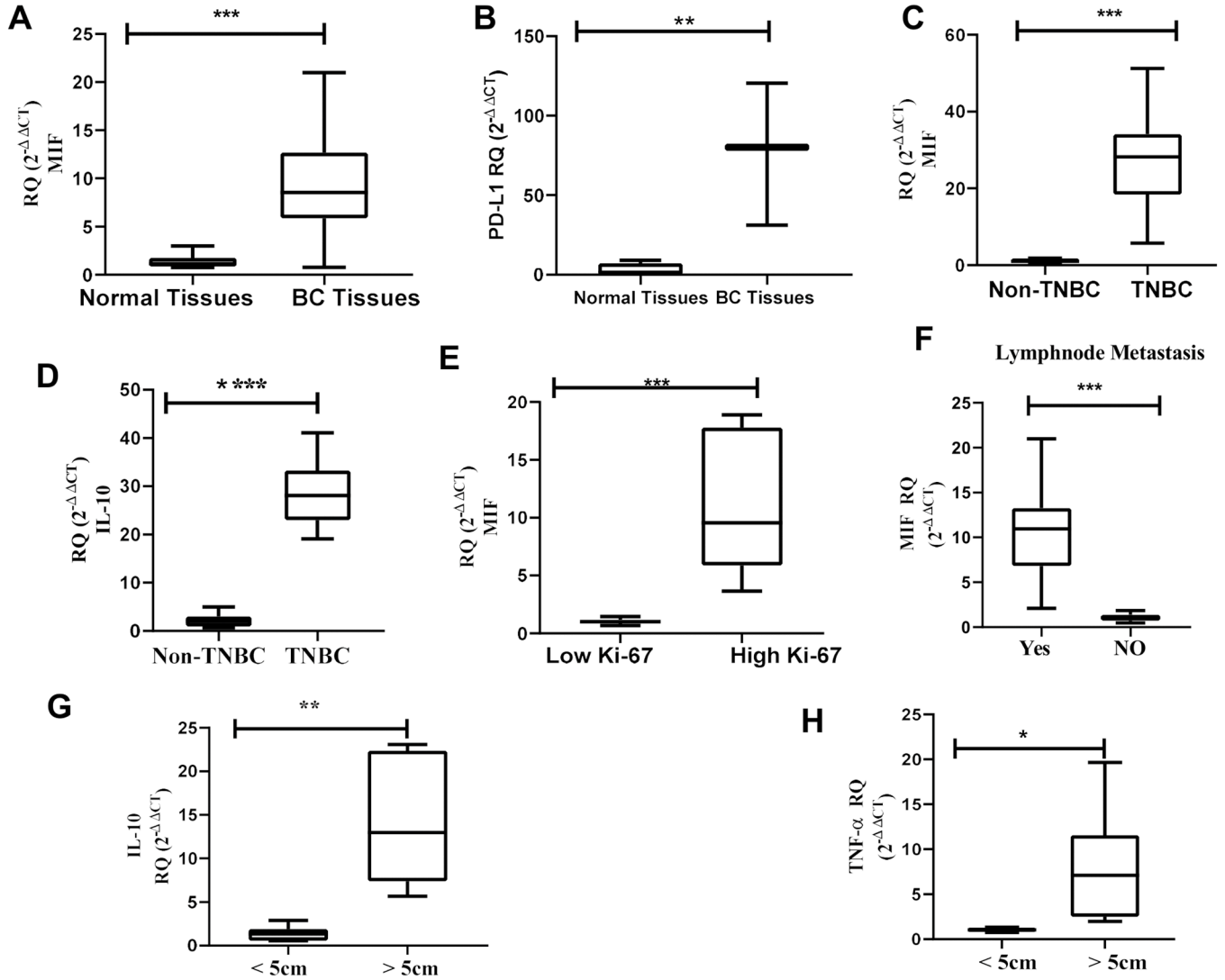

Fig. 2. Expression profiles of the selected markers (MIF, PD-L1, TNF-α & IL-10) in BC and TNBC Patients. (A-B) The expression of MIF and PD-L1 in BC tissues relative to normal ones. (C-D) The expression of MIF and IL 10 in TNBC patients ($n = 10$) relative to non-TNBC patients ($n = 20$). (E-F) The correlation between MIF expression and high Ki-67 values or lymph node metastasis, respectively. (G-H) The correlation between IL-10 or TNF-α and the tumor size, respectively. The expression of all markers was quantified by qRT-PCR and normalized to 18 s rRNA as an internal control. Statistical analysis was performed by a non-parametric unpaired student-*t*-test using GraphPad Prism software 8.3, and data is expressed as mean ± SEM. (*); p value < 0.01, (***); p value

mediators such as IL-10, TNF-α and MIF as well as immune checkpoint proteins such as PD-1/PD-L1 [75–77]. Hence, it could be understood that single-target treatment modality will never achieve satisfactory outcomes creating a pressing need for more rounded, multi-target or multi-functional strategies. Moreover, ncRNAs are strongly involved in tuning the immuno-oncogenic profile of TNBC [77–82]. Nonetheless, natural biomaterials have been recently shown to potentially possess intrinsic immunomodulatory features [55]. Consequently, this study focused on finding alternative approaches to the classical immuno-therapeutic agents via utilization of an engineered hybrid nano-particulate system, a repurposed drug (metformin) and photo-immunomodulation using ce-6.

NPs exhibiting mean particle sizes in the range of 50–150 nm were selected. The rationale of selecting this particle size range is to ensure a long circulation time and an increased accumulation in tumors via the enhanced permeability and retention (EPR) effect as well as a reduced renal clearance [83–85]. In view of the effect of NP composition on their physicochemical properties, a low C:L ratio corresponded to medium-sized CLNPs (CLNP1, CLNP2 & CLNP3). As this ratio increased, particle size decreased resulting in small-sized NPs (CLNP4 & CLNP5). Further increase in C:L ratio resulted in particle size enlargement (CLNP6 & CLNP7). A similar observation was recorded in a study by Khan *et al.*, which was explained based on an optimum ratio required to maintain a compatible interaction between both components; the positively charged amine groups in the chains of chitosan and the negatively charged phosphate groups in lecithin. Any composition above or below

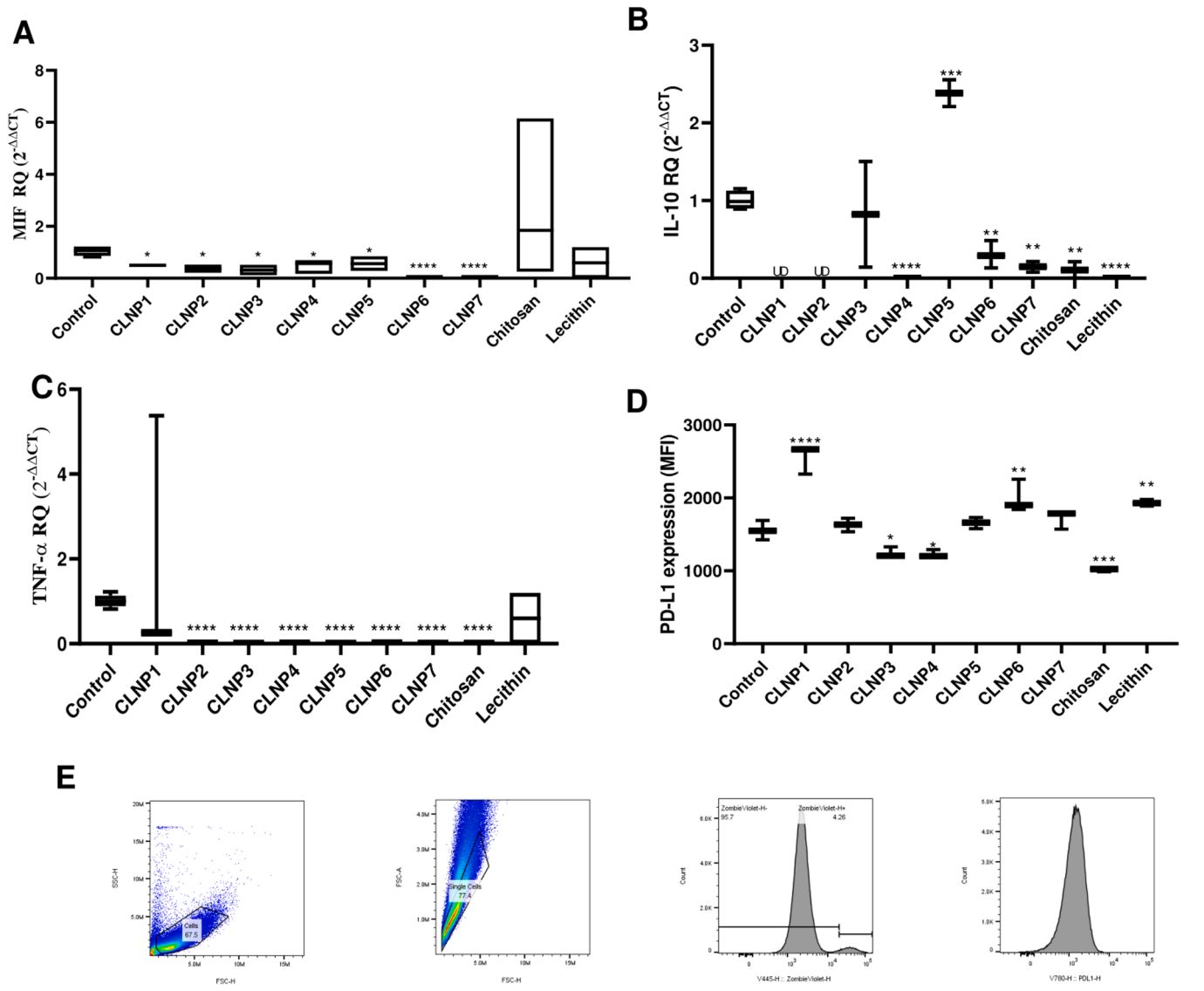

Fig. 3. The effect of CLNPs on the immunosuppressive microenvironment of TNBC. (A-C) Expression levels of MIF, IL-10, and TNF-α, respectively, quantified using q-RT-PCR in MDA-MB-231 cells after treatment with IC_{50} conditions of CLNPs, chitosan or 1 mg/ml of lecithin for 48 hr. (D) The expression level of PD-L1 quantified using single-parameter flow cytometry in MDA-MB-231 cells treated with the IC_{50} conditions of CLNPs, chitosan or 1 mg/ml of lecithin for 48 h depicted as median fluorescence intensity (MFI). (E) The gating approach used in the single-parameter flow cytometry investigation. From left to right, the first panel shows the cell population that was chosen according to the forward scatter height (FSC—H) against side scatter height (SSC—H) plot. The second panel showing FSC—H versus FSC area (FSC-A) plot was used to exclude doublet cells. Zombie violet positive population (dead cells) was excluded in the third panel. Finally, the single parameter histogram of PD-L1 is shown in the fourth panel. Statistical analysis was performed by one-way ANOVA using GraphPad Prism software 8.3, and data is expressed as mean ± SEM. UD; undetermined, (*); p value <0.05, (**); p value< 0.01, (***); p value <0.001, (****); p value <0.0001.

the optimum ratio resulted in the disruption of this interaction and accordingly an enlargement in particle size [86]. Similarly, the surface charge of NPs was dictated by their composition. In our case, positively charged chitosan interacts with negatively charged phospholipids in lecithin. This explains the trend of decrease in negativity, increase in positivity as C:L ratio increases [87].

Regarding the intracellular uptake, it is well established that the extent of NP uptake is determined by their size, shape, surface charge, and surface chemistry [88]. In this current study, an interplay between different factors seemed to control the extent of NPs uptake. For instance, CLNP1, CLNP2 and CLNP3, which are only different in their composition (C:L ratio) exhibited a similar accumulation tendency in MDA-MB-231 cells. While CLNP4 showed the highest extent of uptake due to its smaller size, higher surface positivity, composition or a combination of different parameters [89]. However, when C:L ratio was further increased in CLNP5, while particle size was maintained, this advantage was lost. Therefore, only the lower content of phospholipids could explain the decrease in intracellular accumulation in this case. Regarding CLNP6 & CLNP7, which also had the same size (approximately 140 nm), showed an opposite pattern. Whereas CLNP7 which exhibited a higher C:L ratio, showed almost 4-fold higher intracellular accumulation than CLNP6, this could be due to the positivity or rigidity that is a known property of polymers [90].

On the clinical level, 30 breast biopsies were resected from BC patients for the evaluation of the expression of MIF, PD-L1, TNF-α, and IL-10 from tumor biopsies relative to their normal counterparts. Results showed a significant upregulation of all the markers in BC tissues in comparison to normal tissues. These findings are consistent with previous studies [91–94]. Upon patient stratification, higher MIF and IL-10 expression levels were observed in TNBC over non-TNBC patients, correlating with the negative status of ER and PR [80,95,96]. Moreover, our results showed a correlation between MIF expression and lymph

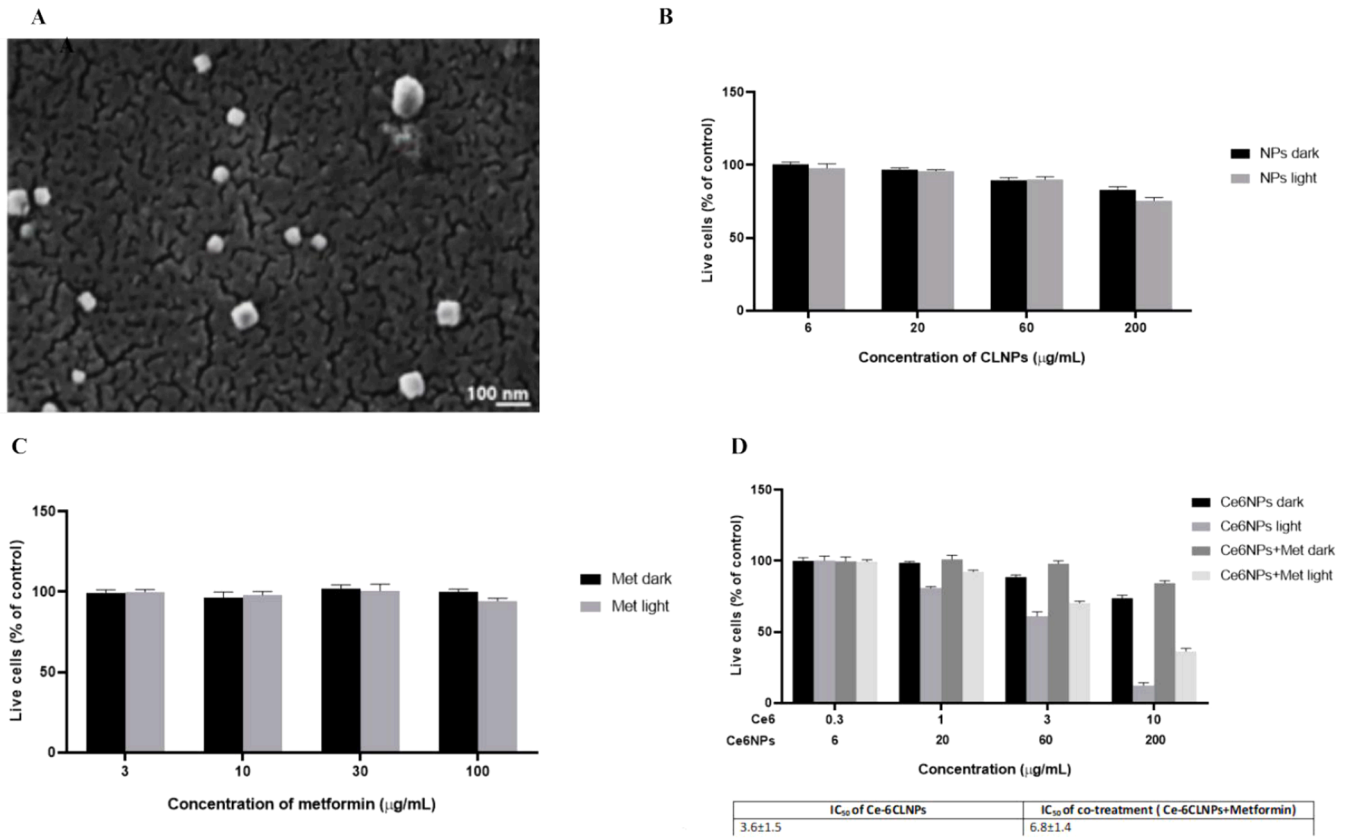

Fig. 4. Surface morphology,& Cell viability of Ce-6CLNPs in MDA-MB-231 breast cancer cells.
(A)SEM micrographs of ce-6 CLNPS by Carl Zeiss Supra 55 FE-SEM at electron high tension (EHT) of 5 kV and magnification 10–20 k x.(B-D) Cell viability of MDA-MD-231 exposed to ce-6CLNPs, or ce-6CLNPs in combination with metformin in the absence of light exposure PDT monotherapy and PDT + metformin after being exposed to home-made LED for 40 s Each experiment was repeated at least three times. Statistical analysis was performed by one-way ANOVA followed by Tukey's post-hoc test using GraphPad Prism software 8.3, and data is expressed as mean ± SEM. ns; not significant, (****);p value <0.0001.

node metastasis and elevated Ki-67 in consistence with previous studies indicating that MIF may play a role in the progression of cancer to a more aggressive and metastatic phenotype [97,98], suggesting that MIF and IL-10 overexpression were shown to be associated with worse prognosis in TNBC when compared to other hormonal subtypes as previously reported [99,100]. As a result, our findings suggest that MIF, TNF-α, IL-10 and PD-L1 can be regarded as potential biomarkers and therapeutic targets.

After validating the altered expression of the therapeutic targets in BC patients, MDA-MB-231 cells were treated with engineered drugless CLNPs, chitosan and lecithin solutions to explore the effect of the interplay of the physicochemical properties on regulating the immunosuppressive milieu of TNBC. The desirable immunomodulatory effects obtained upon exposure to lecithin (downregulation of IL-10) could trace back to its phospholipid content. Changes in the phospholipid pool has been previously shown to orchestrate an array of immune responses [101]. The impact of chitosan solution was rather different; it could significantly downregulate IL-10, TNF-α in addition to PD-L1. Numerous reports demonstrated the ability of chitosan to modulate the expression of different markers in a context-dependent manner [102,103].

Regarding the CLNPs, each formulation exhibited a different impact on the expression of the immunosuppressive cytokines and the immune checkpoint protein (PD-L1) based on its physicochemical properties such as particle size and material composition (C:L ratio). It is worth noting that nanoscale materials have different features and act differently than their bulk counterparts, potentially due to their large surface area to volume ratio [104]. CLNP4, which exhibited a small particle size of 60 nm and intermediate C:L ratio of 1:1, was regarded as the most promising formulation, as it reduced the expression of all immunosuppressive markers in this study. This could be related to the physicochemical properties on one hand and to the subcellular localization on the other [105,106]. Therefore, these results suggest that combining both biomaterials in a hybrid system maximizes the benefits of the resulting NPs.

We were interested in pursuing these findings in a more translational approach, therefore we used CLNP4 to encapsulate ce-6 (ce-6CLNPs) to demonstrate their inherent potential to modulate the TIME milieu of TNBC patients. Ce-6CLNPs exhibited a small particle size (100 nm), acceptable PDI (0.4), high EE% (99.5) and positive surface charge (ZP = 23.9 mV), sufficient for maintaining a good standing stability. NP formulations with zeta potentials greater than +20 mV or less than −20 mV are considered stable because they have enough electrostatic repulsion to remain in solution preventing the aggregation of the NPs [107].

Upon application of PDT to MDA-MB-231 cells, an efficient anticancer effect was established with an IC_{50} of 6.6 μg/mL. PDT is a three-component (light, PS and cellular or tissue oxygen) treatment modality which mediates robust anticancer effects through the generation of ROS [108–111]. Yet, the combination of PDT with a non-cytotoxic concentration of metformin produced a non-significant increase in the viability with an IC_{50} of 7.7 μg/mL. However, upon evaluating the relative efficacy of the mono- or combination therapy on the molecular level, the combination was found to be less efficient. A significant loss of the impact of PDT on relieving the immunosuppressive TIME and the immune checkpoint signaling was observed in the combination therapy. Despite that growing evidence has elaborated on the potential anticancer and immunomodulatory potential of metformin, a lot of studies came to different conclusions [59,63]. In fact, the impact of metformin in cancer is rather a controversy.

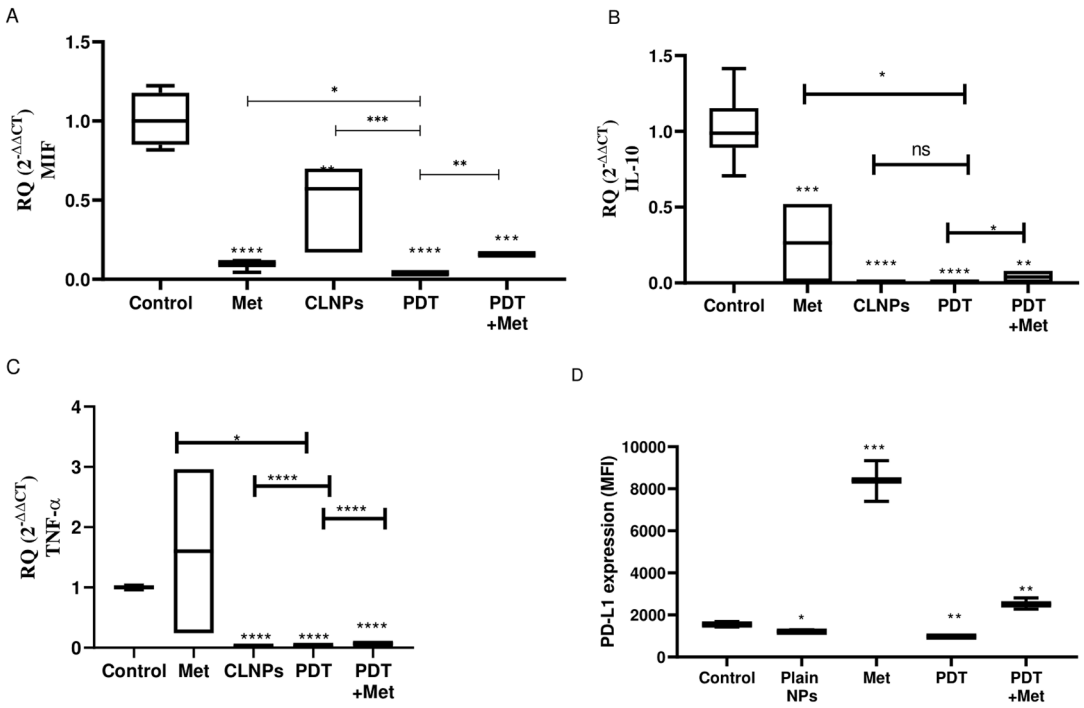

Fig. 5. The effect of ce-6CLNPs ± metformin on the immunosuppressive microenvironment of TNBC. (A-C) Expression levels of MIF, IL-10, and TNF-α, respectively, quantified using q-RT-PCR in MDA-MB-231 cells after treatment with IC_{50} conditions of Ce-6CLNP and non-toxic concentration of Metformin for 48 hr. (D) The expression level of PD-L1 quantified using single-parameter flow cytometry in MDA-MB-231 cells treated with the IC_{50} conditions of Ce-6CLNPs, and non-toxic concentration of for 48 h depicted as median fluorescence intensity (MFI).

This study explored the potential regulatory role of ce-6CLNPs-mediated PDT on ncRNAs; the tumor suppressor miR-30a-5p [112] and the oncogenic MALAT-1 [7,113]. Upon evaluation of the interaction of miR-30a-5p and MALAT-1 in TNBC cell line, it was confirmed that both ncRNAs form a ceRNA network; in which the forced expression of miR-30a-5p reduced MALAT-1 levels, while the knockdown of MALAT-1 resulted in an overexpression of miR-30a-5p. Moreover, the impact of MALAT1/miR-30a-5p ceRNA network on the quadruple targets employed in this study; TNF-α, IL-10, MIF and PDL1 has been established and validated by our group [74]. Results showed that the upregulation of miR-30a-5p resulted in a significant reduction in TNF-α and IL-10 expression. On the other hand, upon knocking down MALAT-1, a significant downregulation of MIF and PD-L1 expression was observed. These findings collectively suggest that miR-30a-5p is an immune-activator miRNA in TNBC that suppresses immune-suppressive cytokines such as MIF, TNF-α, and IL-10 and immune checkpoint such as PD-L1.

Furthermore, miR-30a-5p is shown to be a dominant player in the miR-30a-5p/MALAT1 regulatory axis. Interestingly, PDT-treated TNBC cells have been shown a significant alteration in the miR-30a-5p/MALAT1 network. Ce6-CLNP4-mediated PDT tipped the balance towards the tumor suppressor and immune activator, miR-30a-5p over the oncogenic lncRNA MALAT-1. Thess findings support the recently introduced impact of PDT on the ncRNA milieu in oncology [114,115] .

Although our *in-vitro* findings strongly support the efficacy of this multimodal therapeutic strategy, the absence of its *in-vivo* validation represents one of the major limitations of the current study. Further work should be focused on the establishment of a TNBC mouse model to explore how non-medicated and medicated CLNPs affect tumor-immune interactions. These *in-vivo* studies, including biodistribution and efficacy assessments, are currently ongoing and will be reported in a separate publication.

Conclusion

In this *in-vitro* study, CLNPs demonstrated inherent ability to modulate the TIME of TNBC cells by suppressing the immunosuppressive mediators (MIF, TNF-α and IL-10) and the immune checkpoint protein (PD-L1). The immunomodulatory role of CLNPs was shown to be unique. CLNP4 was then nominated for use as a PS carrier system. Ce6-CLNP4-mediated photodynamic reaction resulted in a potent anticancer effect in MDA-MB-231. Despite that the combination with metformin yielded no significant difference on the functional level, it resulted in a deterioration of the effect on the molecular level. A significant loss of the impact of PDT on relieving the immunosuppressive TIME and the immune checkpoint signaling was observed in the combination therapy. Moving forward with the monotherapy, an interesting impact of the Ce6-CLNP4-mediated PDT on the miR-30a-5p/ MALAT-1 ceRNA network was observed. PDT mediated by Ce6-CLNP4 tilted the balance in favor of the tumor suppressor and immune activator miR-30a-5p over the oncogenic lncRNA MALAT-1. This study sheds a new light on the role of engineered non-medicated CLNPs and ce-6CLNPs (PDT) in modulating the immunosuppressive milieu of TNBC cells. It also adds emphasis on the role of miR-30a-5p as a tumor suppressor in TNBC, as well as its involvement in the MALAT-1 circuit and their impact on MIF, PD-L1, TNF-α, and IL-10. This *in-vitro* study brings about new evidence supporting the paradigm shift in the way we perceive nanomaterials and encourages their use as actives rather than as inert delivery systems. This paves the way for the design and synthesis of novel NPs capable of simultaneously alleviating the immunosuppressive cytokine storm and decreasing the expression of immune checkpoint proteins.

CRediT authorship contribution statement

Asmaa Ramzy: Writing – original draft, Methodology, Formal analysis, Data curation. **Mohammad Abdel-Halim:** Writing – review & editing, Methodology, Formal analysis. **Tamer Manie:** Writing – review & editing, Resources, Formal analysis, Data curation. **Noha M. Elemam:**

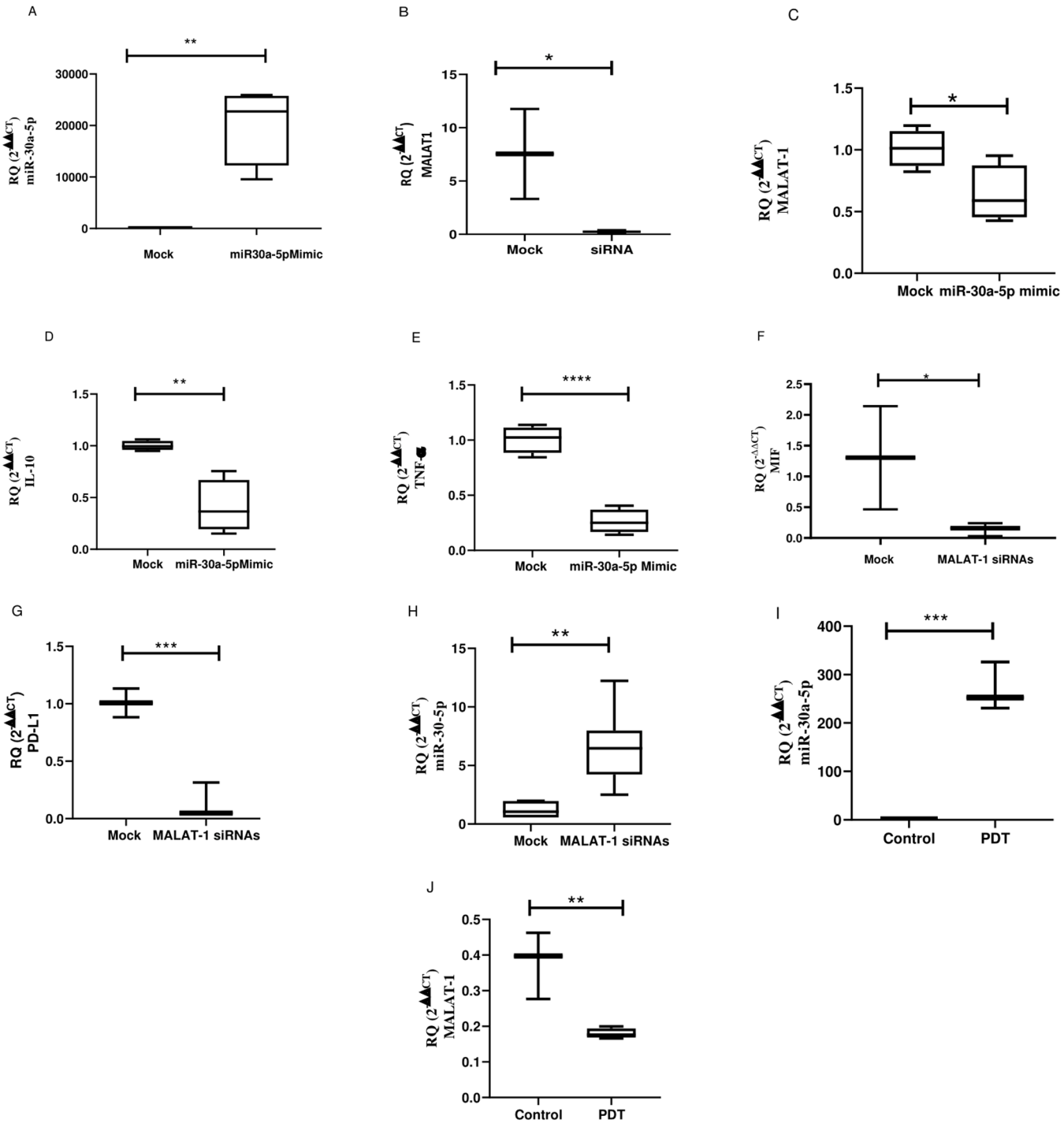

Fig. 6. Interplay of miR-30a-5p, MALAT1, and ce6CLNP4-Mediated PDT: Transcript Dynamics in MDA-MB-231 TNBC Cell Lines.MDA-MB-231 cells were transfected with oligonucleotides of miR-30a-5p mimics (A) and MALAT-1 siRNAs (B). To confirm efficient transfection, miR-30a-5p and MALAT-1 were quantified 48 hrs post transfection using qRT-PCR. miR-30a-5p expression was analyzed in MDA-MB-231 using qRT-PCR, and normalized to RNU6B as an internal control. Upon transfection of miR-30a-5p in MDA-MB-231, MALAT1 siRNAs (C), IL-10 (D) and TNF-α (E) expression level. MIF (F) and PDL1 (G) levels were assessed using qRT-PCR and normalized to β-actin as an internal control. While miR-30a-5p was assessed using qRT-PCR and normalized to RNU6B as an internal control (H). miR-30a-5p (I) and MALAT-1 (J) expression upon exposure to ce6CLNP4 mediated PDT at IC60 conditions of 3.6 μg/mL. mRNA expression was analyzed in MDA-MB-231 using qRT-PCR, and normalized to RNU6B as an internal control. Statistical analysis performed by GraphPad Prism software 8.3. ns; not significant, (*);P value <0.05, (**); p value< 0.01, (***); p value <0.001,(****);p value <0.0001.

Writing – review & editing, Methodology, Investigation, Formal analysis. **Samar Mansour:** Writing – review & editing, Supervision. **Rana A. Youness:** Writing – review & editing, Writing – original draft, Validation, Supervision, Project administration, Funding acquisition, Formal analysis, Data curation, Conceptualization. **Aya Sebak:** Writing – review & editing, Writing – original draft, Validation, Supervision, Project administration, Methodology, Investigation, Funding acquisition, Formal analysis, Data curation, Conceptualization.

Declaration of competing interest

All authors declare no conflict of interest

Ethics approval and consent to participate

This study strictly adhered to ethical guidelines established by the National Cancer Institute, Faculty of Pharmacy and Biotechnology at the German University in Cairo, and the Declaration of Helsinki. Written informed consent was obtained from all patients (Ethical Approval Number: PTC-2020–10-SMH).

Consent for publication

All authors have read and agreed to submit the final version of the manuscript for publication.

Availability of data and materials

Not applicable.

Funding

The Science, Technology & Innovation Funding Authority (STDF) in collaboration with the Egyptian Knowledge Bank (EKB) is providing open access funding. This work was financially supported by a grant (no.43254) from the Science, Technology & Innovation Funding Authority (STIFA).

Acknowledgements

Not applicable.

Data availability

All data used in this study is presented within the main article and supplementary materials.

Supplementary materials

Supplementary material associated with this article can be found, in the online version, at doi:10.1016/j.tranon.2025.102365.

References

[1] B.D. Lehmann, et al., Refinement of triple-negative breast cancer molecular subtypes: implications for neoadjuvant chemotherapy selection, PLoS One 11 (6) (2016) e0157368.
[2] M. Abdel-Latif, R.A. Youness, Why natural killer cells in triple negative breast cancer? World J. Clin. Oncol. 11 (7) (2020) 464–476.
[3] R.A. Assal, et al., A novel epigenetic strategy to concurrently block immune checkpoints PD-1/PD-L1 and CD155/TIGIT in hepatocellular carcinoma, Transl. Oncol. 45 (2024) 101961.
[4] R.A. Youness, et al., A comprehensive insight and In silico analysis of CircRNAs in hepatocellular carcinoma: a step toward ncRNA-based precision medicine, Cells (15) (2024) 13.
[5] G.N. Al-Jussani, et al., Expression of PD-L1 using SP142 CDx in triple negative breast cancer, Ann. Diagn. Pathol 51 (2021) 151703.
[6] P. Garcia-Teijido, et al., Tumor-infiltrating lymphocytes in triple negative breast cancer: the future of immune targeting, Clin. Med. Insights Oncol 10 (Suppl 1) (2016) 31–39.
[7] M. Abdel-Latif, et al., MALAT-1/p53/miR-155/miR-146a ceRNA circuit tuned by methoxylated quercitin glycoside alters immunogenic and oncogenic profiles of breast cancer, Mol. Cell. Biochem 477 (4) (2022) 1281–1293.
[8] R.M. Abdallah, et al., Hindering the synchronization between miR-486-5p and H19 lncRNA by Hesperetin halts breast cancer aggressiveness through tuning ICAM-1, Anticancer Agents. Med. Chem 22 (3) (2022) 586–595.
[9] Y. Fan, S. He, The characteristics of tumor microenvironment in triple negative breast cancer, Cancer Manag. Res 14 (2022) 1–17.
[10] R.-A. SOLIMAN, et al., Uncoupling tumor necrosis factor-α and interleukin-10 at tumor immune microenvironment of breast cancer through miR-17-5p/MALAT-1/H19 circuit, BIOCELL 46 (3) (2022) 769–783.
[11] P. Lotfinejad, et al., PD-L1 silencing inhibits triple-negative breast cancer development and upregulates T-cell-induced pro-inflammatory cytokines, Biomed. Pharmacother 138 (2021) 111436.
[12] A. Ramzy, et al., 134P Drugless nanoparticles tune-up immune components at triple negative breast cancer tumor microenvironment milieu, Annals. Oncol. 32 (2021) S1435.
[13] H. Conroy, L. Mawhinney, S.C. Donnelly, Inflammation and cancer: macrophage migration inhibitory factor (MIF)–the potential missing link, QJM 103 (11) (2010) 831–836.
[14] M. Esquivel-Velazquez, et al., The role of cytokines in breast cancer development and progression, J. Interferon. Cytokine. Res 35 (1) (2015) 1–16.
[15] H. Narasimhan, et al., Tumor necrosis factor-alpha (TNFalpha) stimulate triple-negative breast cancer stem cells to promote intratumoral invasion and neovasculogenesis in the liver of a xenograft model, Biol. (Basel) (10) (2022) 11.
[16] J.R. Hwang, et al., Upregulation of CD9 in ovarian cancer is related to the induction of TNF-α gene expression and constitutive NF-κb activation, Carcinogenesis 33 (1) (2012) 77–83.
[17] Y. Qiao, et al., AP-1 is a key regulator of proinflammatory cytokine TNFalpha-mediated triple-negative breast cancer progression, J. Biol. Chem 291 (10) (2016) 5068–5079.
[18] J.X. Wang, et al., Lactic acid and an acidic tumor microenvironment suppress anticancer immunity, Int. J. Mol. Sci 21 (21) (2020) 8363.
[19] A. Mantovani, P. Allavena, A. Sica, F. Balkwill, Cancer-related inflammation, Nature 454 (7203) (2008) 436–444.
[20] M.C. Heckel, et al., Human breast tumor cells express IL-10 and IL-12p40 transcripts and proteins, but do not produce IL-12p70, Cell Immunol. 266 (2) (2011) 143–153.
[21] K.-Y. Chen, et al., Contribution of interleukin-10 genotype to triple negative breast cancer risk, Anticancer Res. 41 (5) (2021) 2451–2457.
[22] N.M. Elemam, et al., Pharmacogenomic and epigenomic approaches to untangle the enigma of IL-10 blockade in oncology, Expert Rev. Mol. Med 26 (2024) e1.
[23] M.K.A. El-Aziz, et al., Decoding hepatocarcinogenesis from a noncoding RNAs perspective, J. Cell Physiol 238 (9) (2023) 1982–2009.
[24] T. Abaza, et al., Emerging role of circular RNAs in Hepatocellular carcinoma immunotherapy, Int. J. Mol. Sci (22) (2023) 24.
[25] S. Djebali, et al., Landscape of transcription in human cells, Nature 489 (7414) (2012) 101–108.
[26] H. Nafea, et al., Dual targeting of H(2)S synthesizing enzymes; cystathionine β-synthase and cystathionine γ-lyase by miR-939-5p effectively curbs triple negative breast cancer, Heliyon 9 (10) (2023) e21063.
[27] S.H. Wang, et al., The lncRNA MALAT1 functions as a competing endogenous RNA to regulate MCL-1 expression by sponging miR-363-3p in gallbladder cancer, J. Cell Mol. Med 20 (12) (2016) 2299–2308.
[28] N.A. Selem, et al., Let-7a/cMyc/CCAT1/miR-17-5p circuit re-sensitizes atezolizumab resistance in triple negative breast cancer through modulating PD-L1, Pathol. Res. Pract 248 (2023) 154579.
[29] W.F. Li, et al., Overexpression of microRNA-30a-5p inhibits liver cancer cell proliferation and induces apoptosis by targeting MTDH/PTEN/AKT pathway, Tumour. Biol 37 (5) (2016) 5885–5895.
[30] W. Li, et al., Downregulation of β3 integrin by miR-30a-5p modulates cell adhesion and invasion by interrupting Erk/Ets-1 network in triple-negative breast cancer corrigendum in/10.3892/ijo. 2021.5169, Int. J. Oncol. 48 (3) (2016) 1155–1164.
[31] R.Y. Mekky, et al., MALAT-1: immunomodulatory lncRNA hampering the innate and the adaptive immune arms in triple negative breast cancer, Transl. Oncol 31 (2023) 101653.
[32] Y. Miao, et al., Clinical significance of long non-coding RNA MALAT1 expression in tissue and serum of breast cancer, Ann. Clin. Lab. Sci 46 (4) (2016) 418–424.
[33] C. Jin, et al., Reciprocal regulation of hsa-miR-1 and long noncoding RNA MALAT1 promotes triple-negative breast cancer development, Tumor. Biol. 37 (6) (2016) 7383–7394.
[34] Y.A. ZeinElAbdeen, A. AbdAlSeed, R.A. Youness, Decoding insulin-like growth factor signaling pathway from a non-coding RNAs perspective: a step towards precision oncology in breast cancer, J. Mammary Gland Biol. Neoplasia 27 (1) (2022) 79–99.
[35] Y. Pan, et al., Long non-coding MALAT1 functions as a competing endogenous RNA to regulate vimentin expression by sponging miR-30a-5p in hepatocellular carcinoma, Cell Physiol. Biochem 50 (1) (2018) 108–120.
[36] Z. Xiping, et al., Roles of MALAT1 in development and migration of triple negative and her-2 positive breast cancer, Oncotarget 9 (2) (2018) 2255–2267.
[37] S.A. Fahmy, et al., Molecular engines, therapeutic targets, and challenges in pediatric brain tumors: a special emphasis on hydrogen sulfide and RNA-based nano-delivery, Cancer. (Basel) (21) (2022) 14.
[38] R.A. Youness, et al., A snapshot of photoresponsive liposomes in cancer chemotherapy and immunotherapy: opportunities and challenges, ACS. Omega 8 (47) (2023) 44424–44436.
[39] S.A. Fahmy, et al., Emerging tendencies for the nano-delivery of gambogic acid: a promising approach in oncotherapy, RSC Adv 14 (7) (2024) 4666–4691.
[40] A.H. Soliman, et al., Phytochemical-derived tumor-associated macrophage remodeling strategy using Phoenix dactylifera L. boosted photodynamic therapy in melanoma via H19/iNOS/PD-L1 axis, Photodiagnosis. Photodyn. Ther 44 (2023) 103792.
[41] W. Gao, et al., Drug self-delivery nanorods enhance photodynamic therapy of triple-negative breast cancer by inhibiting oxidative phosphorylation, Int. J. Pharm 621 (2022) 121775.

[42] L.E. Ibarra, et al., Selective photo-assisted eradication of triple-negative breast cancer cells through aptamer decoration of doped conjugated polymer nanoparticles, Pharmaceutics 14 (3) (2022).
[43] A. Oniszczuk, et al., The potential of photodynamic therapy (PDT)-experimental investigations and clinical use, Biomed. Pharmacother 83 (2016) 912–929.
[44] Y.H. Moon, et al., Efficient preparation of highly pure chlorin e6 and its photodynamic anti-cancer activity in a rat tumor model, Oncol. Rep 22 (5) (2009) 1085–1091.
[45] D. Fong, C.D. Hoemann, Chitosan immunomodulatory properties: perspectives on the impact of structural properties and dosage, Fut. Sci. OA 4 (1) (2018) FSO225.
[46] A.M. Weiss, et al., Immunostimulatory polymers as adjuvants, immunotherapies, and delivery systems, Macromolecules 55 (16) (2022) 6913–6937.
[47] J. Ding, Y. Guo, Recent advances in Chitosan and its derivatives in cancer treatment, Front. Pharmacol 13 (2022) 888740.
[48] T. Nandgude, R. Pagar, Plausible role of chitosan in drug and gene delivery against resistant breast cancer cells, Carbohydr. Res 506 (2021) 108357.
[49] C. Li, et al., Recent progress in drug delivery, Acta. Pharm. Sin. B 9 (6) (2019) 1145–1162.
[50] E. Katsuta, O.M. Rashid, K. Takabe, Clinical relevance of tumor microenvironment: immune cells, vessels, and mouse models, Hum. Cell 33 (4) (2020) 930–937.
[51] M.K. Amin, J.S. Boateng, Enhancing stability and mucoadhesive properties of chitosan nanoparticles by surface modification with sodium alginate and polyethylene glycol for potential oral Mucosa vaccine delivery, Mar. Drugs 20 (3) (2022).
[52] N. Morin-Crini, et al., Applications of chitosan in food, pharmaceuticals, medicine, cosmetics, agriculture, textiles, pulp and paper, biotechnology, and environmental chemistry, Environ. Chem. Lett 17 (2019) 1667–1692.
[53] D. Lee, K. Powers, R. Baney, Physicochemical properties and blood compatibility of acylated chitosan nanoparticles, Carbohydr. Polym 58 (2004) 371–377.
[54] U.N. Das, Bioactive lipids in age-related disorders, Adv. Exp. Med. Biol 1260 (2020) 33–83.
[55] A. Ramzy, et al., Drugless nanoparticles tune-up an array of intertwined pathways contributing to immune checkpoint signaling and metabolic reprogramming in triple-negative breast cancer, Biomed. Mater 18 (1) (2022).
[56] L. Dai, et al., Structural characterization, formation mechanism and stability of curcumin in zein-lecithin composite nanoparticles fabricated by antisolvent co-precipitation, Food Chem 237 (2017) 1163–1171.
[57] M.M. Khan, et al., Folate targeted lipid chitosan hybrid nanoparticles for enhanced anti-tumor efficacy, Nanomedicine 28 (2020) 102228.
[58] J. Langedijk, et al., Drug repositioning and repurposing: terminology and definitions in literature, Drug Discov. Today 20 (8) (2015) 1027–1034.
[59] R.J. Shaw, et al., The kinase LKB1 mediates glucose homeostasis in liver and therapeutic effects of metformin, Science 310 (5754) (2005) 1642–1646.
[60] M.K. Asiedu, et al., Patient- and cell type-specific heterogeneity of metformin response, Basic. Clin. Pharmacol. Toxicol 122 (2) (2018) 214–222.
[61] S. Bayraktar, et al., Effect of metformin on survival outcomes in diabetic patients with triple receptor-negative breast cancer, Cancer 118 (5) (2012) 1202–1211.
[62] K.K. Tsilidis, et al., Metformin does not affect cancer risk: a cohort study in the U. K. Clinical practice research datalink analyzed like an intention-to-treat trial, Diabetes Care 37 (9) (2014) 2522–2532.
[63] C.J. Currie, C.D. Poole, E.A. Gale, The influence of glucose-lowering therapies on cancer risk in type 2 diabetes, Diabetologia 52 (9) (2009) 1766–1777.
[64] P. Calvo, et al., Chitosan and chitosan/ethylene oxide-propylene oxide block copolymer nanoparticles as novel carriers for proteins and vaccines, Pharm. Res 14 (10) (1997) 1431–1436.
[65] A. Ahmed Sebak, et al., Nano-mediated PDT as a multifunctional immunomodulatory agent in the intricate milieu of Melanoma, Adv. Therap. (2024).
[66] J.R. Masters, G.N. Stacey, Changing medium and passaging cell lines, Nat. Protoc 2 (9) (2007) 2276–2284.
[67] A. Ramzy, et al., Multitarget, multiagent PLGA nanoparticles for simultaneous tumor eradication and TME remodeling in a melanoma mouse model, Drug. Deliv. Transl. Res (2023).
[68] S.L. Jacques, How tissue optics affect dosimetry of photodynamic therapy, J. Biomed. Opt 15 (5) (2010) 051608.
[69] R. Hibst, et al., Thermal effects of white light illumination during microsurgery: clinical pilot study on the application safety of surgical microscopes, J. Biomed. Opt 15 (4) (2010) 048003.
[70] I. Gomaa, et al., Liposomal delivery of ferrous chlorophyllin: a novel third generation photosensitizer for in vitro PDT of melanoma, Photodiagnosis. Photodyn. Ther 18 (2017) 162–170.
[71] R.A. Youness, et al., Contradicting interplay between insulin-like growth factor-1 and miR-486-5p in primary NK cells and hepatoma cell lines with a contemporary inhibitory impact on HCC tumor progression, Growth. Factors 34 (3–4) (2016) 128–140.
[72] Y.J. Ahn, et al., Colorimetric detection of endogenous hydrogen sulfide production in living cells, Spectrochim. Acta. A. Mol. Biomol. Spectrosc 177 (2017) 118–124.
[73] R.A. Youness, et al., MicroRNA-486-5p enhances hepatocellular carcinoma tumor suppression through repression of IGF-1R and its downstream mTOR, STAT3 and c-myc, Oncol. Lett 12 (4) (2016) 2567–2573.
[74] A. Ramzy, et al., 40P MALAT-1/miR-30a-5p competing endogenous (ceRNA) network releases the brakes of immune surveillance in breast cancer through its quadruple targets: PD-L1, MIF, IL-10 and TNF-α, Annal. Oncol. 32 (2021) S1357–S1358.
[75] L. Chocarro de Erauso, et al., Resistance to PD-L1/PD-1 Blockade Immunotherapy. A tumor-intrinsic or tumor-extrinsic phenomenon? Front. Pharmacol (2020) 11.
[76] C.M. Fares, et al., Mechanisms of resistance to Immune checkpoint blockade: why does checkpoint inhibitor immunotherapy not work for all patients? Am. Soc. Clin. Oncol. Educ. Book 39 (2019) 147–164.
[77] C. Han Li, Y. Chen, Small and long non-coding RNAs: novel targets in perspective cancer therapy, Curr. Genomics 16 (5) (2015) 319–326.
[78] X.X. Deng, et al., Taraxacum mongolicum extract inhibited malignant phenotype of triple-negative breast cancer cells in tumor-associated macrophages microenvironment through suppressing IL-10 /STAT3 / PD-L1 signaling pathways, J. Ethnopharmacol 274 (2021) 113978.
[79] K. Greish, S. Taurin, M.A. Morsy, The effect of adjuvant therapy with TNF-alpha on animal model of triple-negative breast cancer, Ther. Deliv. 9 (5) (2018) 333–342.
[80] M. Charan, et al., Macrophage migration inhibitory factor inhibition as a novel therapeutic approach against triple-negative breast cancer, Cell Death Dis 11 (9) (2020) 774.
[81] D.F. Tavares, et al., Immunotherapy using PD-1/PDL-1 inhibitors in metastatic triple-negative breast cancer: a systematic review, Oncol. Rev 15 (2) (2021) 497.
[82] Y. Pan, et al., Long non-coding MALAT1 functions as a competing endogenous RNA to regulate vimentin expression by sponging miR-30a-5p in hepatocellular carcinoma, Cellul. Physiol. Biochem 50 (2018) 108–120.
[83] W.B. Liechty, N.A. Peppas, Expert opinion: responsive polymer nanoparticles in cancer therapy, Eur. J. Pharm. Biopharm 80 (2) (2012) 241–246.
[84] H. Hillaireau, P. Couvreur, Nanocarriers' entry into the cell: relevance to drug delivery, Cell. Mol. Life. Sci 66 (17) (2009) 2873–2896.
[85] J. Wu, The enhanced permeability and retention (EPR) effect: the significance of the concept and methods to enhance its application, J. Pers. Med (8) (2021) 11.
[86] M. Khan, et al., Co-delivery of curcumin and cisplatin to enhance cytotoxicity of cisplatin using lipid-chitosan hybrid nanoparticles, Int. J. Nanomedicine 15 (2020) 2207–2217.
[87] I. Henriksen, et al., Interactions between liposomes and chitosan II: effect of selected parameters on aggregation and leakage, Int. J. Pharm 146 (1997) 193–203.
[88] T. Dou, et al., Cellular uptake and transport characteristics of chitosan modified nanoparticles in Caco-2 cell monolayers, Int. J. Biol. Macromol 138 (2019) 791–799.
[89] A.A. Sebak, Limitations of pegylated nanocarriers: unfavourable physicochemical properties, biodistribution patterns and cellular and subcellular fates, Int. J. Appl. Pharmac. (2018).
[90] A.A. Sebak, et al., Distinct proteins in protein corona of nanoparticles represent a promising venue for endogenous targeting - part I: in vitro release and intracellular uptake perspective, Int. J. Nanomed. 15 (2020) 8845–8862.
[91] I. Cotzomi-Ortega, et al., Autophagy inhibition in breast cancer cells induces ROS-mediated MIF expression and M1 macrophage polarization, Cell Signal 86 (2021) 110075.
[92] M. Bou Zerdan, et al., Triple negative breast cancer: updates on classification and treatment in 2021, Cancer. (Basel) 14 (5) (2022).
[93] S.R.K. Murthy, et al., BCL2A1 regulates Canady Helios Cold plasma-induced cell death in triple-negative breast cancer, Sci. Rep 12 (1) (2022) 4038.
[94] N.J. Toney, et al., Tumor-B-cell interactions promote isotype switching to an immunosuppressive IgG4 antibody response through upregulation of IL-10 in triple negative breast cancers, J. Transl. Med 20 (1) (2022) 112.
[95] C. Chavey, et al., Oestrogen receptor negative breast cancers exhibit high cytokine content, Breast Cancer Res 9 (1) (2007) R15.
[96] B.Changkija Hamidullah, R. Konwar, Role of interleukin-10 in breast cancer, Breast Cancer Res. Treat 133 (1) (2012) 11–21.
[97] C. Greenwood, et al., Stat1 and CD74 overexpression is co-dependent and linked to increased invasion and lymph node metastasis in triple-negative breast cancer, J. Proteomics 75 (10) (2012) 3031–3040.
[98] S.H. Madani, et al., The correlation between Ki-67 with other prognostic factors in breast cancer: a study in Iranian patients, Ind. J. Med. Paediatr. Oncol. 37 (2) (2016) 95–99.
[99] X. Wang, Y. Lin, Tumor necrosis factor and cancer, buddies or foes? Acta. Pharmacol. Sin 29 (11) (2008) 1275–1288.
[100] González-Garza, M., D. Cruz-Vega, and C. Bernal, IL10 as cancer biomarker. 2020.
[101] V.B. O'Donnell, J. Rossjohn, M.J. Wakelam, Phospholipid signaling in innate immune cells, J. Clin. Invest 128 (7) (2018) 2670–2679.
[102] D.P. Vasconcelos, et al., Macrophage polarization following chitosan implantation, Biomaterials 34 (38) (2013) 9952–9959.
[103] C.R. Almeida, et al., Impact of 3-D printed PLA- and chitosan-based scaffolds on human monocyte/macrophage responses: unraveling the effect of 3-D structures on inflammation, Acta. Biomater 10 (2) (2014) 613–622.
[104] G. Guisbiers, S. Mejía-Rosales, F.Leonard Deepak, Nanomaterial properties: size and shape dependencies, 2012 180976.
[105] M. Elsabahy, K.L. Wooley, Cytokines as biomarkers of nanoparticle immunotoxicity, Chem. Soc. Rev 42 (12) (2013) 5552–5576.
[106] D. Fong, C. Hoemann, Chitosan immunomodulatory properties: perspectives on the impact of structural properties and dosage, Fut. Sci. Open Access (2017) 4.
[107] T.C. Prathna, N. Chandrasekaran, A. Mukherjee, Studies on aggregation behaviour of silver nanoparticles in aqueous matrices: effect of surface functionalization and matrix composition, Colloid. Surfac. A 390 (1) (2011) 216–224.
[108] D.E. Dolmans, D. Fukumura, R.K. Jain, Photodynamic therapy for cancer, Nat. Rev. Cancer 3 (5) (2003) 380–387.

[109] Y. Tomizawa, J. Tian, Photodynamic therapy for unresectable cholangiocarcinoma, Dig. Dis. Sci 57 (2) (2012) 274–283.
[110] J. Choi, et al., Light-triggered photodynamic nanomedicines for overcoming localized therapeutic efficacy in cancer treatment, Adv. Drug. Deliv. Rev (2022) 114344.
[111] C.H. Ma, et al., Photodynamic therapy in combination with chemotherapy, targeted, and immunotherapy As a successful therapeutic approach for advanced gastric adenocarcinoma: a case report and literature review, Photobiomodul. Photomed. Laser. Surg 40 (5) (2022) 308–314.
[112] L. Li, et al., miR-30a-5p suppresses breast tumor growth and metastasis through inhibition of LDHA-mediated Warburg effect, Cancer Lett 400 (2017) 89–98.
[113] A. Dawoud, et al., Circular RNAs: new layer of complexity evading breast cancer heterogeneity, Noncod. RNA Res 8 (1) (2023) 60–74.
[114] W. Zhou, et al., lncRNA TINCR participates in ALA-PDT-induced apoptosis and autophagy in cutaneous squamous cell carcinoma, J. Cell Biochem 120 (8) (2019) 13893–13902.
[115] S.M. El-Daly, M.L. Abba, A.M. Gamal-Eldeen, The role of microRNAs in photodynamic therapy of cancer, Eur. J. Med. Chem 142 (2017) 550–555.